Asymptotic approximation of long time solution for low temperature filtration combustion *

Grigori Chapiro [a], Alexei A. Mailybaev [b], Aparecido J. de Souza [c], Dan Marchesin [d] and Johannes Bruining [e]

[a] *UFJF, Juiz de Fora, Brazil, grigori@ice.ufjf.br.*
[b] *Moscow State University, Moscow, Russia, mailybaev@imec.msu.ru.*
[c] *UFCG, Campina Grande, Brazil, cido@dme.ufcg.edu.br.*
[d] *IMPA, Rio de Janeiro, Brazil, marchesi@fluid.impa.br.*
[e] *TU Delft, Delft, The Netherlands, j.bruining@tudelft.nl.*

Abstract

There is renewed interest using combustion for the recovery of medium viscosity oil. We consider the combustion process when air in injected into the porous medium containing some fuel and inert gas. Commonly the reaction rate is negligible at low temperatures, hence the possibility of oxygen breakthrough. In this case the oxygen gets in contact with the fuel in the downstream zone leading to slow reaction. For applications in the field this assumption may fail due to low-temperature oxidation reactions, which are relatively fast at low temperatures, as well as due to very small heat losses. We focus on the case when the reaction is active for all temperatures, but heat losses are negligible. For a combustion model that includes heat and mass balance equations, we develop a method for calculating the wave profile in the form of an asymptotic expansion and derive its zero- and first-order approximations. This wave profiles appears to be different from wave profiles analyzed in other papers, where only the reaction at highest temperatures was taken into account. The combustion wave has a long decaying tail in the field, but not in the laboratory. This is so because heat losses must be very small for the long tail to form. Numerical simulations were performed in order to validate our asymptotic formulae.

Keywords: *Filtration combustion, Traveling wave, Singular perturbation, Low temperature oxidation, Asymptotic expansions.*
AMS classification: 80A25, 76S05.

1 Introduction

In this paper we consider the combustion process when air in injected into porous medium containing initially some fuel (e.g., oil) and inert gas. There are many analytical studies of steady co-flow combustion waves in high-temperature regimes, e.g., [2, 3, 4, 5, 14, 15, 17]. The method in these papers usually explores strong nonlinearity of the Arrhenius factor in the reaction rate, which allows neglecting the reaction rate as soon as the temperature decreases [19]. This method is valid provided that most of the reaction occurs at the highest temperatures. One of the consequences

*This work was supported in part by: CNPq under Grants: 301564/2009-4, 472923/2010-2, 490707/2008-4, 314583/2009-2, 478668/2007-4; FAPERJ under Grants: E-26/110.972/2008, E-26/102.723/2008, E-26/112.220/2008, E-26/110.337/2010; FAPEMIG.

of this assumption is that oxygen is not consumed completely at the highest temperatures and its breakthrough becomes possible. In such a case the oxygen gets in contact with fuel downstream of the fast reaction zone, leading to slow reaction in the downstream zone. In many practical applications this reaction rate is extremely low, and the generated heat dissipates to the surrounding media. This is the main reason for neglecting reaction at low temperatures, e.g., in laboratory experiments. However, for field applications there are low-temperature oxidation reactions, which are relatively fast; as well as heat losses are very small.

In this paper, we focus on the latter case, i.e., when the reaction is active for all temperatures, but heat losses are negligible. For a combustion model that includes heat and mass balance equations, we develop a method for computing the wave profile in the form of an asymptotic expansion. In particular, we derive formulae for zero- and first-order approximations of the profile. It turns out that the wave has a long decaying tail. Due to its long span, such a combustion wave may exist in field experiments, but not in laboratory conditions, because this tail occurs only if heat losses are very small. To justify our results, we perform direct numerical simulations of the original system. The results of the numerical simulations are in perfect agreement with our asymptotic formulae.

The paper is organized as follows. In Section 2, we describe the physical model for in-situ combustion and its dimensionless form. In Section 3, we describe the solution of the problem as a wave sequence. In Section 4, we derive the zero-order asymptotic expression for the combustion wave profile. In Section 5, numerical computations and simulations are carried out for the case of low temperature oil oxidation. The results are summarized in the Conclusion section. In the Appendix we present the details about asymptotic expansion for the wave profile and compute its zero and first order terms using the singular perturbation method.

2 The model

We study one-dimensional flows possessing a combustion wave in the case when the oxidizer (air with oxygen) is injected in the porous medium, see Figure 1. The medium contains initially a fuel that is essentially immobile and does not vaporize, and a non-reactive gas. This is the case for solid fuel, or for liquid fuel at low saturations so it does not move. In our simplified model, we assume that only a small part of the available space is occupied by the fuel, so that changes of porosity in the reaction are negligible. We assume that the temperature of solid and gas is the same (local thermal equilibrium). Heat losses are neglected, which is reasonable for in-situ combustion in field conditions. We also assume that pressure variations are small compared to prevailing pressure.

The model with time coordinate t and space coordinate x includes the heat balance equation (1), the molar balance equations for total gas (2), oxygen (3), immobile fuel (4), and the ideal gas law (5):

$$C_m \frac{\partial T}{\partial t} + \frac{\partial (c_g \rho u (T - T_{res}))}{\partial x} = \lambda \frac{\partial^2 T}{\partial x^2} + Q_r W_r \tag{1}$$

$$\varphi \frac{\partial \rho}{\partial t} + \frac{\partial (\rho u)}{\partial x} = (\mu_g - \mu_o) W_r, \tag{2}$$

$$\varphi \frac{\partial (Y\rho)}{\partial t} + \frac{\partial (Y \rho u)}{\partial x} = D\varphi \frac{\partial}{\partial x} \left(\rho \frac{\partial Y}{\partial x} \right) - \mu_o W_r, \tag{3}$$

$$\frac{\partial \rho_f}{\partial t} = -\mu_f W_r, \tag{4}$$

$$T = P/(\rho R). \tag{5}$$

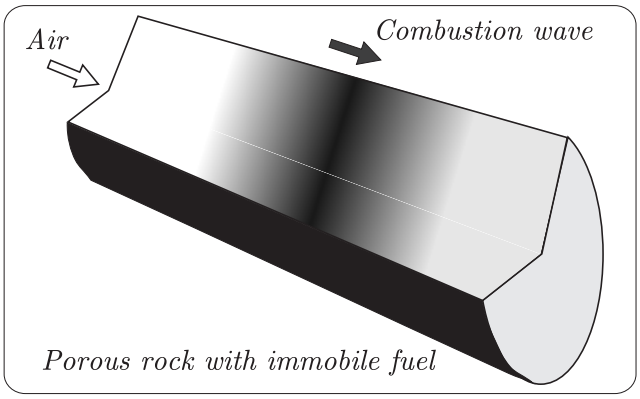

Figure 1: Sketch of in-situ combustion.

Table 1: Dimensional parameters for in-situ combustion and their typical values.

Symbol	*Physical quantity*	*Value*	*Unit*
T_{res}	Initial reservoir temperature	370	[K]
C_m	Heat capacity of porous medium	$2 \cdot 10^6$	[J/m^{3}K]
c_g	Heat capacity of gas	27.42	[J/mole K]
λ	Thermal conductivity of porous medium	0.87	[J/(m s K)]
Q_r	Immobile fuel combustion enthalpy at T_{res}	$4 \cdot 10^5$	[J/mole]
φ	Porosity	0.3	[·]
D	Gas diffusion coefficient	$2 \cdot 10^{-6}$	[m^2/s]
E_r	Activation energy	58000	[J/mole]
k_p	Pre-exponential parameter	500	[1/s]
R	Ideal gas constant	8.314	[J/(mole K)]
P	Prevailing pressure (1 atm)	101325	[Pa]
u_{inj}	Darcy velocity of injected gas (200 m/day)	$2.3 \cdot 10^{-3}$	$[m/s]$
Y_{inj}	Oxygen molar fraction in injected gas	0.21	[·]
ρ_f^{res}	Initial molar density of fuel	372	[mole/m^3]

Here T $[K]$ is the temperature, ρ $[mole/m^3]$ is the molar density of gas, Y $[mole/mole]$ is the oxygen molar fraction in the gas, u $[m/s]$ is the Darcy velocity of gas, ρ_f $[mole/m^3]$ is the molar concentration of immobile fuel. The system parameters together with their typical values are given in Table 1. These parameters are assumed to be constant (neglecting the dependence on temperature, gas composition, etc.), an assumption that was already used in (1).

In the combustion reaction, μ_f moles of immobile fuel react with μ_o moles of oxygen and generate μ_g moles of gaseous products and, possibly, unreactive solid products. For simplicity, we consider the case $\mu_f = \mu_o = \mu_g = 1$ as, e.g., in the reaction $C + O_2 \rightarrow CO_2$. The reaction rate W_r will be taken as

$$W_r = k_p Y \rho_f \exp\left(-\frac{E_r}{RT}\right), \tag{6}$$

where typical values of k_p and E_r also are given in Table 1.

The variables to be found are the temperature T, the molar concentration of immobile fuel ρ_f, the molar fractions of oxygen Y, and the Darcy velocity u.

In some works, e.g. [16], the system (1)–(5) is written in terms of mass densities instead of molar densities. It comes with two problems. First, one has to take into account that molar mass depends on gas mixture composition. The second problem is related to the term $c_g\rho$ in (1), which is the average heat capacity of the gases in the mixture at constant pressure. As O_2 and CO_2 are linear molecules, they have the same number of degrees of freedom and their molar heat capacity (at constant pressure) is practically the same. When the reaction can be regarded as being $C+O_2 \rightarrow CO_2$, the total number of moles in the gas does not change during the reaction. Therefore, as O_2 reacts and is replaced by the same number of moles of CO_2, the average molar heat capacity of the mixture stays (practically) constant. This is not the case if the specific heat of the mixture is written in terms of mass rather than in terms of moles, see e.g. [6].

2.1 Dimensionless equations

The equations are non-dimensionalized by introducing dimensionless dependent and independent variables (denoted by tildes) as ratios of the dimensional quantities and reference quantities (denoted by stars):

$$\tilde{t} = \frac{t}{t^*},\ \tilde{x} = \frac{x}{x^*},\ \tilde{\theta} = \Delta\tilde{T} = \frac{T - T_{res}}{\Delta T^*},\ \tilde{\rho} = \frac{\rho}{\rho^*},\ \tilde{\rho}_f = \frac{\rho_f}{\rho_f^*},\ \tilde{u} = \frac{u}{u^*},\ \tilde{Y} = \frac{Y}{Y^*}. \tag{7}$$

Our choice for reference quantities is

$$\begin{gathered} t^* = \frac{1}{k_p Y_{inj}} \exp\left(\frac{E_r}{RT_{res}}\right),\ v^* = \frac{Y_{inj}\rho^* u_{inj}}{\rho_f^{res}},\ x^* = v^* t^*, \\ \Delta T^* = \frac{Q_r \rho_f^{res}}{C_m},\ \rho^* = \frac{P}{RT_{res}},\ \rho_f^* = \rho_f^{res},\ u^* = u_{inj},\ Y^* = Y_{inj}, \end{gathered} \tag{8}$$

where T_{res} and ρ_f^{res} are the initial reservoir temperature and molar density of fuel, u_{inj} is the injection gas velocity, Y_{inj} is the oxygen molar fraction in the injected gas. In (8), v^* turns out to be the combustion wave speed as it is shown later; t^* is the characteristic time for fuel combustion at the initial reservoir temperature T_{res}; ΔT^* is the deviation of peak temperature from reservoir temperature, for the case of complete combustion of fuel under adiabatic conditions. Typical values for parameters in (8) are presented in Section 5.

Using (7), (8) and omitting the tildes, equations (1)–(6) are written in dimensionless form as:

$$\frac{\partial\theta}{\partial t} + V_T \frac{\partial(\rho u\theta)}{\partial x} = \frac{1}{\mathrm{Pe}_T}\frac{\partial^2\theta}{\partial x^2} + \Phi, \tag{9}$$

$$\frac{\partial\rho}{\partial t} + \sigma\frac{\partial(\rho u)}{\partial x} = 0, \tag{10}$$

$$\frac{\partial(Y\rho)}{\partial t} + \sigma\frac{\partial(Y\rho u)}{\partial x} = \frac{1}{\mathrm{Pe}}\frac{\partial}{\partial x}\left(\rho\frac{\partial Y}{\partial x}\right) - \sigma\Phi, \tag{11}$$

$$\frac{\partial\rho_f}{\partial t} = -\Phi, \tag{12}$$

$$\rho = \theta_0/(\theta + \theta_0), \tag{13}$$

$$\Phi = t^* W_r/\rho_f^* = Y\rho_f \exp\left(\frac{\mathcal{E}}{\theta_0} - \frac{\mathcal{E}}{\theta + \theta_0}\right), \tag{14}$$

with dimensionless constants

$$\mathrm{Pe}_T = \frac{v^* x^* C_m}{\lambda}, \quad V_T = \frac{c_g \rho_f^{res}}{C_m Y_{inj}}, \quad \sigma = \frac{\rho_f^{res}}{\varphi Y_{inj} \rho^*},$$
$$\mathrm{Pe} = \frac{v^* x^*}{D}, \quad \mathcal{E} = \frac{E_r}{RT^*}, \quad \theta_0 = \frac{T_{res}}{T^*}. \tag{15}$$

Here Pe_T and Pe are the Peclet numbers for thermal and mass diffusion; σ is the fuel to oxygen concentration rate; V_T turns out to be the dimensionless thermal wave speed as explained later, $\mathcal{E}$ is the scaled activation energy and θ_0 is the scaled reservoir temperature. Typical values of the quantities in (15) are given in Section 5. The system must be solved with the initial reservoir conditions

$$t = 0,\ x \geq 0: \quad \theta = Y = 0, \quad \rho_f = 1, \tag{16}$$

and the injection conditions

$$t \geq 0,\ x = 0: \quad \theta = 0, \quad Y = u = 1, \quad \rho_f = 0. \tag{17}$$

3 Thermal and combustion waves

The solution of system (9)–(13) with general boundary conditions for large times essentially takes the form of a sequence of waves, which can be thermal, combustion, gas or fuel composition waves, see [16]. Particularly with conditions (16), (17) there are only thermal and combustion waves. In typical in-situ applications, the thermal wave is slower than the combustion wave, see, e.g., [14]. We will consider this case from now on.

In the thermal wave, which is upstream of the combustion wave, the fuel concentration and reaction rate are $\rho_f = \Phi = 0$ (burned state). Assuming that σ is large, which is always the case for gas injection, we can neglect small time-derivative terms in (10) and (11). Then we find that the gas flux and oxygen fraction are constant in the thermal wave and equal to their values at the injection point (17), (13): $\rho u = 1$ and $Y = 1$. The temperature varies in the thermal wave from $\theta = 0$ upstream to $\theta^b > 0$ downstream of the wave. We remark that equation (9) with $\rho u = 1$ and with Φ replaced by zero has a solution in the form of a heat wave, which expands in time due to thermal longitudinal conduction and propagates with speed V_T, see, e.g., [15].

We are looking for the combustion wave as a traveling wave moving with positive speed V. All quantities in the wave depend on the traveling coordinate $\xi = x - Vt$. The limiting states of the combustion wave are

$$\xi \to +\infty: \quad \theta^u = Y^u = 0, \quad u^u > 0, \quad \rho_f^u = 1, \tag{18}$$

$$\xi \to -\infty: \quad \theta^b > 0, \quad Y^b = (\rho u)^b = 1, \quad \rho_f^b = 0, \tag{19}$$

where the superscript u denotes the unburned (downstream) state and the superscript b denotes the burned (upstream) state. Here the state (18) corresponds to the initial reservoir state (16), and the state (19) differs from the injection condition (17) because temperature changes in the thermal wave. The unknown quantities in the combustion wave are θ^b, u^u and the wave speed V.

Traveling wave equations are obtained from (9)–(12) by replacing $\partial/\partial t$ by $-V d/d\xi$ and $\partial/\partial x$ by $d/d\xi$. They become

$$-V\theta' + V_T(\rho u \theta)' = \theta''/\mathrm{Pe}_T + \Phi, \tag{20}$$

$$-V\rho' + \sigma(\rho u)' = 0, \tag{21}$$

$$-V(Y\rho)' + \sigma(Y\rho u)' = (\rho Y')'/\mathrm{Pe} - \sigma\Phi, \tag{22}$$

$$-V\rho_f' = -\Phi, \tag{23}$$

where the prime denotes the derivative with respect to ξ. As it was mentioned before, σ is typically large for gas injection, and it is usual to neglect the small terms $-V\rho'$ and $-V(Y\rho)'$ in (21), (22). Under these simplifications we substitute Φ from (23) into (20), (22) and rewrite (20)–(23) as

$$\begin{aligned}
\left(\theta'/\mathrm{Pe}_T + (V - V_T\rho u)\theta + V\rho_f\right)' &= 0, && (24)\\
(\sigma\rho u)' &= 0, && (25)\\
\left(\rho Y'/\mathrm{Pe} - \sigma Y\rho u - \sigma V\rho_f\right)' &= 0, && (26)\\
V\rho_f' &= \Phi. && (27)
\end{aligned}$$

Integrating (24)–(26) between $-\infty < \xi < \infty$, using (13), (18), (19), and the conditions $\theta' = Y' = 0$ at the limiting states $\xi \to \pm\infty$, we obtain

$$\theta^b = 1/(1 - V_T), \quad u^u = 1, \quad V = 1. \tag{28}$$

Notice that the condition $\theta^b > 0$ is equivalent to the requirement $V_T < 1 = V$, i.e., the thermal wave must be slower than the combustion wave. This condition is typically satisfied due to the large heat capacity of porous rock compared to gas heat capacity, see Eq. (15). Conditions (28) for complete consumption of fuel and oxygen are well known, see, e.g. [15, 16, 17]. These relations are equivalent to the Rankine-Hugoniot conditions for shocks. From now on our goal is to compute the traveling profile of the combustion wave, i.e., the dependence of all variables on ξ.

Integrating (24)–(26) from ξ to ∞ and using (18), (23), (28) yields

$$\begin{aligned}
\theta'/\mathrm{Pe}_T &= 1 - \rho_f - \theta/\theta^b, && (29)\\
u &= 1/\rho = (\theta + \theta_0)/\theta_0, && (30)\\
Y'/(\sigma\mathrm{Pe}) &= (Y + \rho_f - 1)(\theta + \theta_0)/\theta_0. && (31)
\end{aligned}$$

Here (30) was used in the derivation of (29) and (31). Equations (29)–(31) together with (27) determine the traveling wave profile. These equations will be studied numerically in Section 5. In the case of small thermal and mass diffusion, an analytical approach for the computation of the wave profile will be developed in the section that follows.

4 Asymptotic expansion for the combustion wave for small diffusion coefficients

Let us rewrite (29), (31) using $V = 1$ from (28), and (27) using (14). We obtain

$$\begin{aligned}
\epsilon\frac{d\theta}{d\hat{\xi}} &= 1 - \rho_f - \theta/\theta^b, && (32)\\
\epsilon\frac{dY}{d\hat{\xi}} &= \frac{\sigma\mathrm{Pe}}{\mathrm{Pe}_T\theta_0}(Y + \rho_f - 1)(\theta + \theta_0), && (33)\\
\frac{d\rho_f}{d\hat{\xi}} &= Y\rho_f \exp\left(\frac{\mathcal{E}}{\theta^b + \theta_0} - \frac{\mathcal{E}}{\theta + \theta_0}\right), && (34)
\end{aligned}$$

where we introduced the scaled coordinate $\hat{\xi} = \mathrm{Pe}_T\epsilon\xi$ with

$$\epsilon = \frac{1}{\mathrm{Pe}_T}\exp\left(\frac{\mathcal{E}}{\theta_0} - \frac{\mathcal{E}}{\theta^b + \theta_0}\right). \tag{35}$$

The right-hand sides of (32)–(34) do not contain small parameters. In particular, $\sigma \mathrm{Pe}/\mathrm{Pe}_T$ is usually large due to the large values of σ. Therefore, we can look for a solution as an asymptotic expansion, assuming that $\epsilon \ll 1$. This hypothesis is valid in some practically important cases as will be shown in Section 5.

The zero-order approximation in the asymptotic expansion is found by setting $\epsilon = 0$ in equations (32) and (33), which yields

$$\theta = (1-\rho_f)\theta^b, \quad Y = 1-\rho_f. \tag{36}$$

Substituting (36) into (34), we obtain

$$\frac{d\rho_f}{d\hat{\xi}} = (1-\rho_f)\rho_f \exp\left(\frac{\mathcal{E}}{\theta^b+\theta_0} - \frac{\mathcal{E}}{(1-\rho_f)\theta^b+\theta_0}\right). \tag{37}$$

The equation (37) can be solved for $\hat{\xi}$ in terms of ρ_f using the exponential integral function $\mathrm{E}_1(x) = \int_x^\infty t^{-1}e^{-t}dt$ (see [1]) as

$$\hat{\xi} = \hat{\xi}_0 + \mathrm{E}_1(a-\eta)\exp(a-b) - \mathcal{R}e\big(\mathrm{E}_1(b-\eta)\big), \tag{38}$$

where

$$a = \frac{\mathcal{E}}{\theta_0}, \quad b = \frac{\mathcal{E}}{\theta^b+\theta_0}, \quad \eta = \frac{\mathcal{E}}{(1-\rho_f)\theta^b+\theta_0}, \tag{39}$$

and $\hat{\xi}_0$ is an arbitrary constant reflecting translational symmetry of the traveling wave solution. The solution (38), (39) can be verified by substituting into (37). Notice that $b < \eta < a$, so that $b-\eta < 0$ in the second exponential integral function in (38). For negative x the function $\mathrm{E}_1(x)$ has constant imaginary part equal to $-i\pi$, see [1]. Thus the real part of the second E_1 function was taken to cancel this irrelevant imaginary part.

In the original coordinate $\xi = \hat{\xi}/(\mathrm{Pe}_T\epsilon)$, expressions (38), (39) and (35) yield

$$\xi = \mathrm{E}_1(a-\eta) - \mathcal{R}e\big(\mathrm{E}_1(b-\eta)\big)\exp(b-a), \tag{40}$$

where we took $\xi_0 = 0$ for simplicity.

The solution of system (32)–(34) can be represented as an asymptotic series $\theta = \theta^0 + \epsilon\theta^1 + \cdots$, $Y = Y^0 + \epsilon Y^1 + \cdots$ and $\rho_f = \rho_f^0 + \epsilon\rho_f^1 + \cdots$, where $\theta^0(\hat{\xi})$, $Y^0(\hat{\xi})$, $\rho^0(\hat{\xi})$ are zero-order approximations given by (36) and (38), (39). In the Appendix, explicit formulae for the correction terms θ^1, Y^1, ρ_f^1 are derived.

5 Numerical example

In this section we present numerical results by using the values of parameters in Table 1. These values correspond to low temperature oxidation reaction of the oil initially present at low concentration in the reservoir. We count moles of fuel as if each molecule has only one carbon atom. The rate of low temperature oxidation varies a lot among different oils. The reaction rate parameters given in Table 1 are compatible with the experimental data for oil in [11].

As we have shown in Section 4, in order to apply the singular perturbation method to system (29), (31), (27) the parameter ϵ defined in (35) must be small. We verify this condition for practical ranges of the reservoir temperature T_{res} and of the injected gas speed u_{inj}; the results are shown in Figure 2. On the plot, the region II corresponds to the case when $\epsilon < 0.1$.

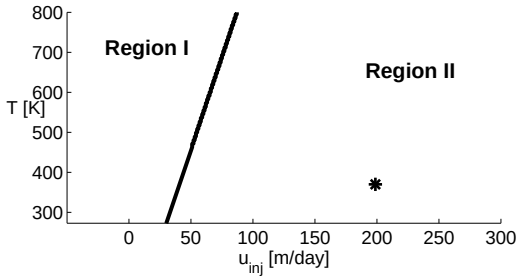

Figure 2: The region II corresponds to points in the parameter space (u_{inj}, T_{res}) where $\epsilon < 0.1$ (other parameters are taken from Table 1). It shows approximately the region, where the asymptotic expansion of Section 4 and of the Appendix is applicable. The solid point corresponds to u_{inj} and T_{res} in Table 1.

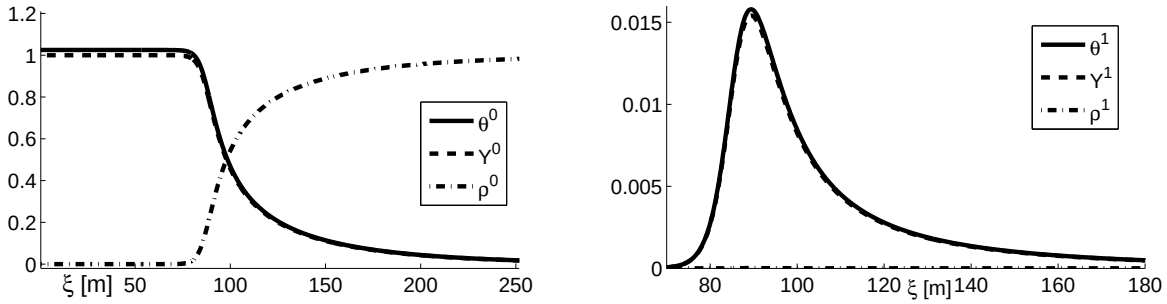

Figure 3: Zero-order approximation of the combustion traveling wave is shown on the left. The first order correction is shown on the right. As the reservoir temperature and injection speed belong to the Region II on Figure 2, the first order correction terms are small. Both figures have horizontal scale in meters; in the vertical scale we show dimensionless quantities θ, Y and ρ_f defined in (7).

Now the results described in previous sections are verified numerically. The parameter values from Table 1 are used. Expressions (8) and (15) yield the following values of reference and dimensionless parameters

$$\begin{gathered} x^* = 62.9\,[m], \quad t^* = 1.463 \cdot 10^6\,[s], \quad \Delta T^* = 74.4\,[K], \\ v^* = 4.3 \cdot 10^{-5}\,[m/s] \quad \text{or} \quad 3.695\,[m/day], \end{gathered} \tag{41}$$

$$\mathrm{Pe}_T = 6180,\ V_T = 0.0243,\ \sigma = 179,\ \mathrm{Pe} = 1344,\ \mathcal{E} = 93.8,\ \theta_0 = 4.97. \tag{42}$$

The zero-order approximation is obtained using (40). Then the first order approximations can be computed as described in the Appendix. The results are presented in Figure 3. Notice that the first-order correction is very small, around 1%, so the approximation is expected to be very accurate. The characteristic length $x^* = 62.9\,[m]$ of the combustion wave is large, since it is determined by the slow reaction at the reservoir temperature, see Eqs. in (8).

In order to solve numerically the original system (9)–(13) we use a splitting method with adaptative time step. For this purpose, we combine equation (10) with (9) and use ρ given by (13) yielding

$$\frac{1}{\mathrm{Pe}_T}\frac{\partial^2\theta}{\partial x^2} - V_T\frac{\partial}{\partial x}\left(\frac{\theta_0 u\theta}{\theta+\theta_0}\right) - \frac{\sigma}{\theta_0}(\theta+\theta_0)^2\frac{\partial}{\partial x}\left(\frac{\theta_0 u}{\theta+\theta_0}\right) + \Phi = 0. \tag{43}$$

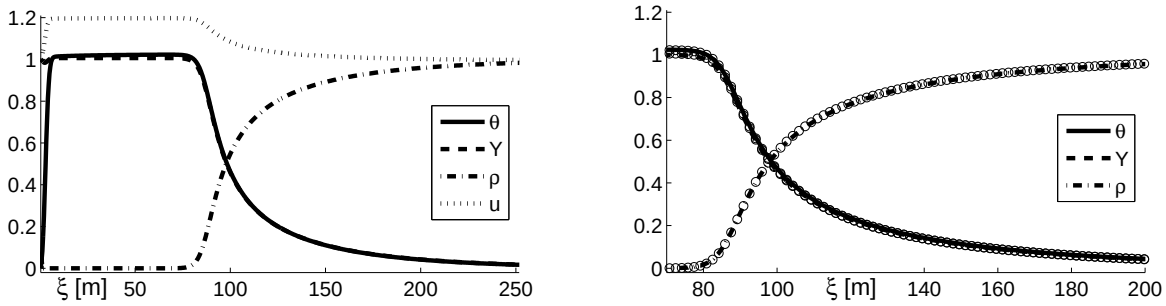

Figure 4: On the left we show numerical simulation results for time $t = 2.6 \cdot 10^6\,[s]$. On the right we compare the combustion wave profile with the zero order asymptotic approximation of the solution. Circles represent numerical simulation results and curves the asymptotic solution. Both figures have horizontal scale in meters; in the vertical scale we show dimensionless quantities θ, Y and ρ_f defined in (7).

Summary of the splitting method:

1. Initialize the variables θ, Y and ρ_f for $t = 0$ as given in (16).

2. Initialize u by direct integration of (43).

3. Apply the classical Crank–Nicolson scheme to equations (9), (11), (12), in order to obtain θ, Y and ρ_f at the new time. Here ρ is given by (13). Use Newton's method to solve the non-linear Crank-Nicolson step taking into account the left boundary Dirichlet conditions (17) and the zero Neumann conditions on the right.

4. As in step **2** calculate u by direct integration of (43).

5. Adapt the size of the future time step using information about convergence of the Newton's method.

• Repeat steps **3, 4** and **5** until the final time is reached.

The simulation results were also confirmed using a hybrid method which combines Crank-Nicolson scheme to solve equations (9), (11), (12) and Box scheme to solve (10), see [6, 7]. On the left side of Figure 4 we plot the simulation results at time $t = 2.6 \cdot 10^6\,[s]$. On the right side of the Figure 4 we compare the combustion wave profile in Figure 3 given by the analytical formulae for the zero-order approximation.

6 Conclusion

We considered the combustion process when air is injected into a porous medium containing immobile fuel and inert gas. Low-temperature oxidation reaction was considered and heat losses where neglected. We assumed that reaction occurs for all temperatures.

A combustion model including heat and mass balance equations for longitudinal flow was considered. We developed a method for computing the traveling wave profile in the form of an asymptotic expansion and derived its zero-order approximation. This wave profiles appears to be different from wave profiles analyzed in other papers, where only the reaction at highest temperatures was taken into account.

One can see from Figs. 3 and 4 that the traveling wave solution contains a long tail in the downstream zone. The reaction rate is essential for all temperatures, as it can be seen by inspecting the oxygen fraction profile. The existence of such a long tail is an essential feature of our solution,

where the heat conduction is assumed to be small and heat losses are negligible. In some cases such as the low-temperature oxidation example considered above, this tail may be reasonably short and the solution is realistic.

When the tail is very long in practice, total heat losses increase, and the heat released by the reaction at low temperatures can be neglected. In such a case, analysis, see e.g., [2, 3, 14, 15, 17], leads to other parameter values for the combustion wave. In particular, oxygen breakthrough phenomenon is possible. We conclude that, in order to identify the appropriate solution method for each particular case, we should take heat losses into account.

7 Appendix: The singular perturbation method

Many different works describe and use singular perturbation methods in order to study multiple scale and stiff problems [12, 13, 18]. Geometric aspects of singularly perturbed differential equation were studied in [10, 13]. More details on the application of this method to our problem are given in [6, 8]. Physical aspects of the resulting approximation are discussed in [9].

Here we apply singular perturbation theory in order to determine a heteroclinic orbit for an autonomous system of ordinary differential equations (32)–(34), which can be written in the general form

$$\begin{cases} \epsilon \dot{\mathbf{x}} = \mathbf{f}(\mathbf{x}, y), \\ \dot{y} = g(\mathbf{x}, y), \end{cases} \tag{44}$$

where ϵ is a small parameter, and the dot denotes the derivative with respect to a real coordinate t. The functions $\mathbf{f} = (f^1, \ldots, f^n)^T$ and g are smooth. The phase space of the system consists of the fast vector $\mathbf{x} \in \mathbb{R}^n$ and slow variable $y \in \mathbb{R}$. We assume that (44) has two isolated equilibria named $(-)$ and $(+)$:

$$\mathbf{f}(\mathbf{x}^-, y^-) = \mathbf{f}(\mathbf{x}^+, y^+) = 0 \quad \text{and} \quad g(\mathbf{x}^-, y^-) = g(\mathbf{x}^+, y^+) = 0, \tag{45}$$

and that

$$g(x, y) \neq 0, \quad \text{for} \quad y \neq y^{\pm}. \tag{46}$$

We are interested in finding a heteroclinic orbit $\mathbf{x}(t), y(t)$ of system (44), which connects $(\mathbf{x}^-, y^-)$ at $t \to -\infty$ to $(\mathbf{x}^+, y^+)$ at $t \to +\infty$. We consider the case $y^- \neq y^+$ when the slow component $y(t)$ undergoes a finite change.

7.1 Zero-order approximation

Let us denote by $\mathbf{x}^0(t), y^0(t)$ the limit $\epsilon \to 0$ of the heteroclinic orbit $\mathbf{x}(t), y(t)$. By taking $\epsilon = 0$ in system (44), we obtain

$$\mathbf{f}(\mathbf{x}^0, y^0) = 0, \tag{47}$$

$$\dot{y}^0 = g(\mathbf{x}^0, y^0). \tag{48}$$

Notice that (47) is a system of n scalar algebraic equations with $n + 1$ unknowns. We assume that this system defines a curve $\mathbf{\Gamma}_0$ in the space $(\mathbf{x}, y)$, which connects the equilibria $(-)$ and $(+)$, see Fig. 5a. We also assume that

$$\det \mathbf{f}_{\mathbf{x}} \neq 0 \ \text{ on } \mathbf{\Gamma}_0, \tag{49}$$

where $\mathbf{f}_{\mathbf{x}} = [\partial \mathbf{f} / \partial \mathbf{x}]$ is the Jacobian matrix of the function $\mathbf{f}(\mathbf{x}, y)$ for fixed y. By the implicit function theorem, equation (47) has a solution $\mathbf{x}^0 = \boldsymbol{\varphi}(y^0)$ such that the curve $\mathbf{\Gamma}_0$ is parametrized as $(\boldsymbol{\varphi}(y^0), y^0)$ for y^0 between y^- and y^+. Of course, $\boldsymbol{\varphi}(y^{\pm}) = \mathbf{x}^{\pm}$.

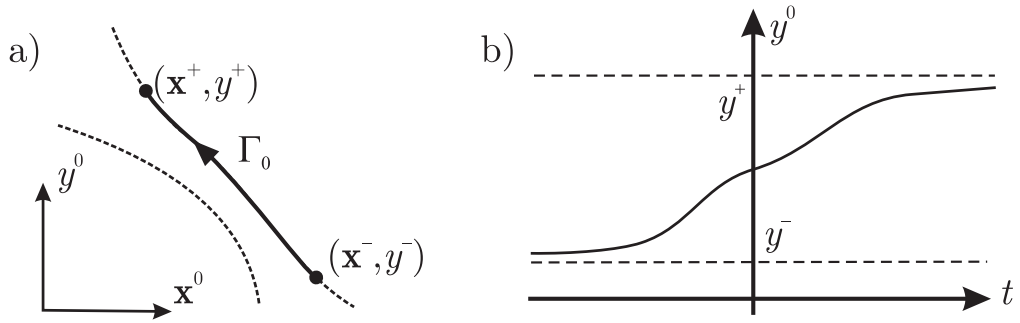

Figure 5: Heteroclinic orbit in zero-order approximation: (a) dependence of $\mathbf{x}^0$ on y^0, (b) dependence of y^0 on t.

By substituting $\boldsymbol{\varphi}(y^0)$ into Eq. (48), we obtain a scalar ODE for y^0:

$$\dot{y}^0 = g(\mathbf{x}^0(y^0), y^0). \tag{50}$$

According to (45), $g(\boldsymbol{\varphi}(y^0), y^0) = 0$ at $y^0 = y^\pm$. Since $g(x, y) \neq 0$, for all $y \neq y^\pm$ there exists a solution $y^0(t)$ such that $y^0 \to y^\pm$ as $t \to \pm\infty$. This solution is a monotone function of t, see Fig. 5b. Equation (50) can be solved forward and backward in t with the initial condition $y^0(0)$ chosen arbitrarily between y^- and y^+ (ambiguity is due to the translational invariance of the solution), which proves:

Proposition 1 *Let us assume that the equation* $\mathbf{f}(\mathbf{x}^0, y^0) = 0$ *determines a curve* $\boldsymbol{\Gamma}_0 = (\boldsymbol{\varphi}(y^0), y^0)$ *connecting the equilibria* $(\mathbf{x}^-, y^-)$ *to* $(\mathbf{x}^+, y^+)$*, satisfying the hypotheses* (46), (49)*. Then the asymptotic heteroclinic solution of system* (44) *in the limit* $\epsilon \to 0$ *is given by* $(\mathbf{x}^0(t) = \boldsymbol{\varphi}(y^0(t)),\ y^0(t))$*, where* $y^0(t)$ *is a solution of equation* (50) *with the initial condition* $y^0(0)$ *chosen arbitrarily between* y^- *and* y^+*.*

7.2 Asymptotic series expansion

The approximate solution given by Proposition 1 is sufficient for many purposes. For example, if ϵ is very small, then the higher order approximations contain little useful information. However, in order to increase the accuracy or estimate the error of approximation, one needs higher-order correction terms. Let us look for a solution of system (44) as an asymptotic power series in ϵ as

$$\mathbf{x}(t) = \mathbf{x}^0(t) + \epsilon\mathbf{x}^1(t) + \epsilon^2\mathbf{x}^2(t) + \cdots, \quad y(t) = y^0(t) + \epsilon y^1(t) + \epsilon^2 y^2(t) + \cdots. \tag{51}$$

By substituting expansions (51) into the functions $\mathbf{f}(\mathbf{x}, y)$, $g(\mathbf{x}, y)$ and expanding them in a power series in ϵ, we obtain

$$\mathbf{f}(\mathbf{x}, y) = \mathbf{f}^0 + \epsilon\mathbf{f}_\mathbf{x}\mathbf{x}^1 + \epsilon\mathbf{f}_y y^1 + \cdots, \quad g(\mathbf{x}, y) = g^0 + \epsilon\mathbf{g}_\mathbf{x}\mathbf{x}^1 + \epsilon g_y y^1 + \cdots. \tag{52}$$

Here $\mathbf{f}^0 = \mathbf{f}(\mathbf{x}^0, y^0)$, $g^0 = g(\mathbf{x}^0, y^0)$ and

$$\mathbf{f}_\mathbf{x} = \begin{bmatrix} \frac{\partial f^1}{\partial x_1} & \cdots & \frac{\partial f^1}{\partial x_n} \\ \vdots & \ddots & \vdots \\ \frac{\partial f^n}{\partial x_1} & \cdots & \frac{\partial f^n}{\partial x_n} \end{bmatrix}, \ \mathbf{f}_y = \begin{bmatrix} \frac{\partial f^1}{\partial y} \\ \vdots \\ \frac{\partial f^n}{\partial y} \end{bmatrix}, \ \mathbf{g}_\mathbf{x} = \begin{bmatrix} \frac{\partial g}{\partial x_1} & \cdots & \frac{\partial g}{\partial x_n} \end{bmatrix}, \ g_y = \left[\frac{\partial g}{\partial y}\right], \tag{53}$$

are functions of t evaluated at $\mathbf{x}^0(t), y^0(t)$. Substituting (51), (52) into (44), we obtain

$$\begin{aligned} \epsilon(\dot{\mathbf{x}}^0 + \epsilon\dot{\mathbf{x}}^1 + \cdots) &= \mathbf{f}^0 + \epsilon\mathbf{f}_{\mathbf{x}}\mathbf{x}^1 + \epsilon\mathbf{f}_y y^1 + \cdots \\ \dot{y}^0 + \epsilon\dot{y}^1 + \cdots &= g^0 + \epsilon\mathbf{g}_{\mathbf{x}}\mathbf{x}^1 + \epsilon g_y y^1 + \cdots . \end{aligned} \tag{54}$$

Since, for any ϵ, $\mathbf{x}(t) \to x^{\pm}$ and $y(t) \to y^{\pm}$ as $t \to \pm\infty$, then the components of expansions (51) must satisfy the following conditions

$$\mathbf{x}^0 \to x^{\pm},\ y^0 \to y^{\pm},\ \mathbf{x}^k \to 0,\ y^k \to 0 \ \text{ as } \ t \to \pm\infty \tag{55}$$

for all integer $k > 0$.

Equating terms with the same power of ϵ, we obtain a series of equations for the unknown functions $\mathbf{x}^k(t)$ and $y^k(t)$. For the zero-order terms we recover equations (47) and (48); thus, $\mathbf{x}^0(t)$ and $y^0(t)$ are given by Proposition 1. Using (50) for the first-order terms in Eq. (54) yields

$$\begin{aligned} \dot{\mathbf{x}}^0 &= \mathbf{f}_{\mathbf{x}}\mathbf{x}^1 + \mathbf{f}_y y^1, \\ \dot{y}^1 &= \mathbf{g}_{\mathbf{x}}\mathbf{x}^1 + g_y y^1. \end{aligned} \tag{56}$$

The solution of this system is given in the following proposition.

Proposition 2 *Let us assume that the hypotheses of Proposition 1 are satisfied. Then the first order terms* $\mathbf{x}^1(t)$ *and* $y^1(t)$ *in the asymptotic expansion* (51) *have the form*

$$\mathbf{x}^1(t) = {\mathbf{f}_{\mathbf{x}}}^{-1}(\dot{\mathbf{x}}^0 - \mathbf{f}_y y^1), \tag{57}$$

$$y^1(t) = g^0 \int_0^t B(\tau)d\tau, \quad B(t) = \mathbf{g}_{\mathbf{x}}{\mathbf{f}_{\mathbf{x}}}^{-2}\mathbf{f}_y. \tag{58}$$

Proof: Let us write (56) as:

$$\dot{\mathbf{x}}^0 - \mathbf{f}_y y^1 = \mathbf{f}_{\mathbf{x}}\mathbf{x}^1, \tag{59}$$

$$\dot{y}^1 = \mathbf{g}_{\mathbf{x}}\mathbf{x}^1 + g_y y^1. \tag{60}$$

Then (57) follows from (59). Using (47), (48) and the chain rule one obtains

$$\dot{\mathbf{x}}^0 = -{\mathbf{f}_{\mathbf{x}}}^{-1}\mathbf{f}_y\dot{y}^0 = -{\mathbf{f}_{\mathbf{x}}}^{-1}\mathbf{f}_y g^0. \tag{61}$$

Substituting this expression into (57) and using the result in (60) one gets

$$\dot{y}^1 = -\mathbf{g}_{\mathbf{x}}{\mathbf{f}_{\mathbf{x}}}^{-1}({\mathbf{f}_{\mathbf{x}}}^{-1}\mathbf{f}_y\, g^0 + \mathbf{f}_y y^1) + g_y y^1. \tag{62}$$

Now using (61) with the chain rule, we find the expression

$$\dot{g}^0 = \mathbf{g}_{\mathbf{x}}\dot{\mathbf{x}}^0 + g_y\dot{y}^0 = -\mathbf{g}_{\mathbf{x}}{\mathbf{f}_{\mathbf{x}}}^{-1}\mathbf{f}_y g^0 + g_y g^0, \tag{63}$$

which can be used in (62) to get

$$\frac{d}{dt}\left(\frac{y^1}{g^0}\right) = -B, \tag{64}$$

where B is defined in (58). Solving (64) one obtains

$$y^1 = cg^0(t) + g^0(t)\int_0^t B(\tau)d\tau, \tag{65}$$

where c is an arbitrary constant. The therm cg^0 is responsible for infinitesimal time-translations of the heteroclinic orbit. Thus, we can take $c = 0$, yielding (58).

Now we have to prove that $\mathbf{x}^1$ and y^1 from (57) and (58) satisfy conditions (55). As $\mathbf{f_x}$ is nonsingular, $B = \mathbf{g_x}{\mathbf{f_x}}^{-2}\mathbf{f}_y$ is a smooth function of t with finite limits as $t \to \pm\infty$. Thus, B is bounded: $|B(t)| < B_{max}$ for some B_{max}. Then y^1 satisfies the inequalities

$$\begin{aligned} |y^1(t)| = \left| g^0(t) \int_0^t B(\tau)d\tau \right| \le B_{max} \left| g^0(t)t \right| \le B_{max} \left(\left| g^0(t)T \right| + \left| g^0(t)(t-T) \right| \right) \le \\ \le B_{max} \left(\left| g^0(t)T \right| + \left| \int_T^t g^0(\tau)d\tau \right| \right) \le B_{max} \left(\left| g^0(t)T \right| + \left| y^0(t) - y^0(T) \right| \right), \end{aligned} \tag{66}$$

where t and T are arbitrary (large) numbers belonging to the interval where $g^0(t)$ is monotone by the hypothesis (46). Now keeping T fixed and taking the limit $t \to \pm\infty$ in (66), we obtain $\lim_{t\to\pm\infty} |y^1(t)| \le B_{max}|y^\pm - y^0(T)|$. Since $y^0(T) \to y^\pm$ as $T \to \pm\infty$, then $y^1 \to 0$ as $t \to \pm\infty$. By using this property in (57), it is straightforward to show that $\mathbf{x}^1 \to 0$ as $t \to \pm\infty$. □

8 Appendix: wave calculations

In the absence of combustion, the source terms representing mass transfer or sensible heat generation containing the factor Φ vanish on the right hand side of system (9)–(13).

$$\frac{\partial\theta}{\partial t} + V_T \frac{\partial(\rho u\theta)}{\partial x} = 0, \tag{67}$$

$$\frac{\partial\rho}{\partial t} + \sigma \frac{\partial(\rho u)}{\partial x} = 0, \tag{68}$$

$$\frac{\partial(Y\rho)}{\partial t} + \sigma \frac{\partial(Y\rho u)}{\partial x} = 0, \tag{69}$$

$$\frac{\partial\rho_f}{\partial t} = 0, \tag{70}$$

$$\rho = \theta_0/(\theta + \theta_0). \tag{71}$$

We open all the derivatives in (67)–(69):

$$\partial_t\theta + V_T(\rho u\partial_x(\theta) + \rho\theta\partial_x(u) + u\theta\partial_x(\rho)) = 0, \tag{72}$$

$$\partial_t\rho + \sigma\rho\partial_x(u) + \sigma u\partial_x(\rho) = 0, \tag{73}$$

$$\rho\partial_t(Y) + Y\partial_t(\rho) + \sigma(Y\rho\partial_x(u) + \rho u\partial_x(Y) + Yu\partial_x(\rho)) = 0, \tag{74}$$

where we used compact notations for derivatives, ∂_x and ∂_t. Isolating $\partial_x u$ from (73) we obtain:

$$\partial_x u = -\frac{\partial_t\rho}{\sigma\rho} - \frac{u\partial_x\rho}{\rho} \tag{75}$$

and substituting it into (72) with ρ from (71):

$$\left[\frac{1}{V_T} + \frac{\theta\theta_0}{\sigma(\theta+\theta_0)^2} \right] \partial_t\theta = -\frac{\theta_0 u}{\theta_0 + \theta}\partial_x\theta. \tag{76}$$

From (73) we have: $\partial_t\rho + \sigma\rho\partial_x(u) = -\sigma u\partial_x(\rho)$, using it in (74) we obtain:

$$\partial_t Y = -\sigma u\partial_x Y. \tag{77}$$

In increasing order, the characteristic speeds of system (70), (75)-(77) and the corresponding characteristic vectors in the state space (θ, Y, ρ_f, u) are:

$$\lambda^{\rho_f} = 0, \qquad (0,0,1,0)^T, \tag{78}$$

$$\lambda^{\theta} = \frac{V_T u \theta_0 \sigma(\theta+\theta_0)}{\sigma(\theta+\theta_0)^2 + \theta\theta_0 V_T}, \qquad (1,0,0,f(u,\theta))^T, \tag{79}$$

$$\lambda^{Y} = \sigma u, \qquad (0,1,0,0)^T, \tag{80}$$

where we omitted the extensive formula for $f(u,\theta)$.

9 Appendix: Solving the integral

One rewrites (37) in integral form:

$$\exp\left(\frac{\mathcal{E}}{\theta_0+\theta_b}\right)(\hat{\xi}-\hat{\xi}_0) = \int_{\hat{\rho}_f}^{\rho_f^0} \exp\left(\frac{\mathcal{E}}{\theta_0+\theta_b(1-\rho_f)}\right)\frac{d\rho_f}{(1-\rho_f)\rho_f} \equiv \bigstar. \tag{81}$$

where $\hat{\rho}_f \in (0,1)$ corresponds to the value $\rho_f^0(\xi_0)$. Variable substitution

$$\eta = \frac{\mathcal{E}}{\theta_0+\theta_b(1-\rho_f)}, \quad d\eta = \frac{\mathcal{E}\theta_b d\rho_f}{(\theta_0+\theta_b(1-\rho_f))^2} = \frac{\eta^2\theta_b}{\mathcal{E}}d\rho_f$$

leads to

$$(1-\rho_f) = \frac{\mathcal{E}-\eta\theta_0}{\theta_b\eta}, \quad \rho_f = \frac{\eta(\theta_0+\theta_b)-\mathcal{E}}{\theta_b\eta}.$$

It follows:

$$\bigstar = \int_{\hat{\eta}}^{\eta^0} e^{\eta}\frac{\theta_b\eta}{\eta(\theta_0+\theta_b)-\mathcal{E}}\frac{\theta_b\eta}{\mathcal{E}-\eta\theta_0}\frac{\mathcal{E}}{\theta_b\eta^2}d\eta = \mathcal{E}\theta_b\int_{\hat{\eta}}^{\eta^0} e^{\eta}\frac{1}{\eta(\theta_0+\theta_b)-\mathcal{E}}\frac{1}{\mathcal{E}-\eta\theta_0}d\eta.$$

Using $a = \mathcal{E}/\theta_0$, $b = \mathcal{E}/(\theta_0+\theta_b)$ we obtain:

$$\bigstar = \frac{\theta_b}{\mathcal{E}(a-b)}\left[a\int_{\hat{\eta}}^{\eta^0}\frac{e^{\eta}d\eta}{\eta/b-1} + b\int_{\hat{\eta}}^{\eta^0}\frac{e^{\eta}d\eta}{1-\eta/a}\right].$$

Using $x = \eta/b - 1$ and $y = 1-\eta/a$ and special Exponential Integral function, see [1], we obtain

$$a\int_{\hat{\eta}}^{\eta^0}\frac{e^{\eta}d\eta}{\eta/b-1} = ab\int_{\hat{x}}^{x^0}\frac{e^{bx+b}dx}{x} = ab\,e^b\int_{\hat{x}}^{x^0}\frac{e^{bx}d(-bx)}{-bx} = \tag{82}$$
$$-ab\,e^b\left[E_1(-bx^0)-E_1(-b\hat{x})\right] = -ab\,e^b\left[E_1(b-\eta^0)-E_1(b-\hat{\eta})\right];$$

$$b\int_{\hat{\eta}}^{\eta^0}\frac{e^{\eta}d\eta}{1-\eta/a} = -ab\int_{\hat{y}}^{y^0}\frac{e^{a-ay}dy}{y} = -ab\,e^a\int_{\hat{y}}^{y^0}\frac{e^{-ay}d(ay)}{ay} = \tag{83}$$
$$ab\,e^a\left[E_1(ay^0)-E_1(a\hat{y})\right] = ab\,e^a\left[E_1(a-\eta^0)-E_1(a-\hat{\eta})\right].$$

Substituting everything into (81) we obtain:

$$e^b(\hat{\xi}-\hat{\xi}_0)\frac{\mathcal{E}(a-b)}{\theta_b} = -ab\,e^b\left[E_1(b-\eta^0)-E_1(b-\hat{\eta})\right] + ab\,e^a\left[E_1(a-\eta^0)-E_1(a-\hat{\eta})\right]$$

$$(\hat{\xi}-\hat{\xi}_0)\frac{\mathcal{E}(a-b)}{ab\,\theta_b} = -\left[E_1(b-\eta^0)-E_1(b-\hat{\eta})\right]+e^{a-b}\left[E_1(a-\eta^0)-E_1(a\,\hat{-}\,\eta)\right]$$

Notice that

$$\frac{\mathcal{E}(a-b)}{ab\,\theta_b}=\frac{\mathcal{E}}{\theta_b}\frac{\mathcal{E}\theta_b}{\theta_0(\theta+\theta_b)}\frac{\theta_0(\theta+\theta_b)}{\mathcal{E}^2}=1.$$

Following

$$\hat{\xi}-\hat{\xi}_0 = -\left[E_1(b-\eta^0)-E_1(b-\hat{\eta})\right]+e^{a-b}\left[E_1(a-\eta^0)-E_1(a-\hat{\eta})\right].$$

Gathering all constants into ξ_0 yields

$$\hat{\xi}=\hat{\xi}_0-E_1(b-\eta^0)+e^{a-b}E_1(a-\eta^0).$$

Notice that $b<\eta<a$, so that $b-\eta<0$ in the exponential integral function. The function $\mathrm{E}_1(x)$ has the constant imaginary part $-i\pi$ for negative x, see [1]. We take the real part of the first E_1 function to cancel this irrelevant imaginary part (compare with (38)).

$$\hat{\xi}=\hat{\xi}_0-\mathrm{Re}\left[E_1(b-\eta^0)\right]+e^{a-b}E_1(a-\eta^0). \tag{84}$$

From (35) we get:

$$\hat{\xi}=\mathrm{Pe}_T\epsilon\xi=\exp\left(\frac{\mathcal{E}}{\theta_0}-\frac{\mathcal{E}}{\theta^b+\theta_0}\right)\xi=e^{a-b}\xi.$$

Using it in (84) we get:

$$\xi=\xi_0-e^{b-a}\mathrm{Re}\left[E_1(b-\eta^0)\right]+E_1(a-\eta^0). \tag{85}$$

Acknowledgment D.M. is indebted to Yucel Akkutlu for discussions and explanations on the physical model of in situ combustion.

References

[1] Abramowitz, M., Stegun, I.: Handbook of mathematical functions with formulas, graphs, and mathematical tables. Dover publications (1964)

[2] Akkutlu, I., Yortsos, Y.: The dynamics of in-situ combustion fronts in porous media. J. of Combustion and Flame **134**, 229–247 (2003)

[3] Aldushin, A., Rumanov, I., Matkowsky, B.: Maximal energy accumulation in a superadiabatic filtration combustion wave. J. of Combustion and Flame **118**, 76–90 (1999)

[4] Aldushin, A., Seplyarsky, B.: Propagation of exothermic reaction in a porous-medium during gas blowing. Sov. Phys. Dokl. **23**, 483–485 (1978)

[5] Bruining, J., Mailybaev, A., Marchesin, D.: Filtration combustion in wet porous medium. SIAM Journal on Applied Mathematics **70**, 1157–1177 (2009)

[6] Chapiro, G.: Gas-solid combustion in insulated porous media. Ph.D. thesis, IMPA (2009). Http://www.preprint.impa.br

[7] Chapiro, G., Hime, G., Mailybaev, A., Marchesin, D., de Souza, A.: Global asymptotic effects of the structure of combustion waves in porous media. In: Hyperbolic Problems: Theory, Numerics, and Applications: Plenary and Invited Talks: Twelfth International Conference on Hyperbolic Problems, June 9-13, 2008, vol. 67, pp. 487–496. AMS (2009)

[8] Chapiro, G., Mailybaev, A.A., Marchesin, D., Souza, A.: Singular perturbation in combustion waves for gaseous flow in porous media. In: Proceedings of XXVI CILAMCE (October, 19-21, 2005). Guarapari, Brasil

[9] Chapiro, G., Marchesin, D.: Non-diffusive combustion waves in insulated porous media. Brazilian Journal of Petroleum and Gas **2**(2), 18–28 (2008)

[10] Fénichel, N.: Geometric singular perturbation theory for ordinary differential equations. Journal of Differential Equations **31**, 53–98 (1979)

[11] Freitag, N., Verkoczy, B.: Low-temperature oxidation of oils in terms of SARA fractions: why simple reaction models don't work. In: Canadian International Petroleum Conference, Calgary, Alberta (2003)

[12] Johnson R., S.: Singular Perturbation Theory, mathematical analytical techniques with applications to engineering. Springer, New York (2005)

[13] Jones, C.: Geometric singular perturbation theory in dynamical systems. Lecture Notes in Math., Springer, Berlin **1609**, 44–118 (1995)

[14] Mailybaev, A.A., Bruining, J., Marchesin, D.: Analysis of in situ combustion of oil with pyrolysis and vaporization. Combustion and Flame (2011). To appear (published online 2010)

[15] Schult, D., Matkowsky, B., Volpert, V., Fernandez-Pello, A.: Forced forward smolder combustion. Combustion and Flame **104**(1-2), 1–26 (1996)

[16] Souza, A.J., Marchesin, D., Akkutlu, I.Y.: Wave sequences for solid fuel adiabatic in-situ combustion in porous media. Comp. Appl. Math **25**(1), 27–54 (2006)

[17] Wahle, C., Matkowsky, B., Aldushin, A.: Effects of gas-solid nonequilibrium in filtration combustion. Combustion Science and Technology **175**, 1389–1499 (2003)

[18] Wasow, W.: Asymptotic expansions for ordinary differential equations. Dover, New York (2002)

[19] Zeldovich, Y.B., Barenblatt, G.I., Librovich, V.B., Makhviladze, G.M.: The mathematical theory of combustion and explosion. Consultants Bureau, New York (1985)